SSRG International Journal of Electrical and Electronics Engineering
ISSN: 2348-8379/ https://doi.org/10.14445/23488379/IJEEE-V11I10P124

Volume 11 Issue 10, 231-248, October 2024

Original Article

Performance Enhancement of Grid Connected Multilevel Inverter Based Wind Energy Conversion System with LVRT Capability Using Optimized Type 2 ANFIS Based DVR

Ch. Sajan[1], P. Satish Kumar[2], Peter Virtic[3]

[1]*University College of Engineering, Osmania University, Hyderabad, Telangana, India.*
[2]*Department of Electrical Engineering, University College of Engineering, Osmania University, Hyderabad, Telangana, India.*
[3]*Faculty of Energy Technology, University of Maribor, Krško, Slovenia.*

[1]*Corresponding Author : sajan4315@gmail.com*

Received: 16 August 2024 Revised: 15 September 2024 Accepted: 17 October 2024 Published: 30 October 2024

Abstract *- A Permanent Magnet Synchronous Generator (PMSG) based Wind Energy Conversion System (WECS) holds significant importance in the realm of Renewable Energy Sources (RES) for several reasons. The permanent magnets in the generator eliminate the need for a separate excitation system, leading to improved efficiency in power conversion. This makes PMSG-based WECS an effective and reliable source of wind energy electricity. The motivation behind the proposed conceptual framework stems from the need to overcome the limitations related to the integration of RES into the power grid, specifically focusing on voltage stability and Low Voltage Ride Through (LVRT) capability of PMSG based WECS. A Dynamic Voltage Restorer (DVR), empowered by an energy storage device, is used to mitigate voltage fluctuations and disturbances. The input DC voltage to the DVR is intricately regulated by a Type 2 Adaptive Neuro Fuzzy Inference System (ANFIS) Controller optimized using the Seagull algorithm, exhibiting intelligent adaptability to dynamic conditions. The rectified output from the WECS transforms an Isolated Flyback converter. Subsequently, a 31-Level Cascaded H-Bridge Multilevel Inverter (CHBMLI) along with a Proportional-Integral (PI) controller aids in generating high-quality AC output. By addressing challenges related to voltage stability and the ability to ride through low-voltage conditions, the proposed work contributes to enhanced grid stability. The use of advanced control techniques, including the Type 2 ANFIS Controller optimized by the Seagull algorithm, adds a layer of intelligent adaptability to changing environmental and grid conditions. A lower Total Harmonic Distortion (THD) Value of 1.29% is shown during the validation of the created system utilizing MATLAB/Simulink, assuring significant LVRT capabilities.*

Keywords *- PMSG, WECS, RES, Low Voltage Ride Through (LVRT), Type 2 Adaptive Neuro Fuzzy Inference System,31-Level CHBMLI, PI.*

1. Introduction

The increasing global commitment to reducing carbon emissions has spurred significant growth in RES adoption, with wind energy emerging as a prominent source owing to its abundance, sustainability and cost-effectiveness [1]. As technology advances, WECS has evolved into a mature solution for large-scale renewable energy generation. However, integrating wind energy into the power grid presents unique challenges, primarily due to the variability and intermittency of wind, which causes fluctuations in power output and voltage instability in the grid [2]. The stability, efficiency and reliability of WECS is assured with the optimal choice of generator. Several types of generators have been employed in wind systems, including Squirrel Cage Induction Generators (SCIG), Doubly-Fed Induction Generators (DFIG), and PMSG [4-6]. The SCIG [7], which is the widely used generator in early wind turbine design, lacks the ability of independent control of reactive power. The DFIG [8], on the other hand, offers enhanced control over both active and reactive power with better grid integration and flexibility. However, it is prone to wear and requires frequent maintenance.

Additionally, it is unsuitable for LVRT applications due to its vulnerability to grid disturbances. The PMSG [9] is comparatively a more advanced technology for WECS with reduced maintenance requirements and superior active and reactive power control. Despite these benefits, PMSG-based WECS are highly sensitive to voltage instability due to the fluctuating nature of wind. This necessitates the use of

advanced Power Conditioning Devices (PCDs) to maintain grid stability, especially under low voltage conditions [10].

Current research in wind energy systems highlights a gap in addressing the limitations of PMSG-based WECS in managing voltage stability under fluctuating wind conditions. A range of PCDs has been employed to manage voltage instability and improve PQ. PCDs like Static Var Compensators (SVC) [11] are widely used to manage reactive power and stabilize voltage levels in the grid. However, it is inept in handling fast voltage fluctuations under severe grid disturbances due to its limited dynamic response capabilities.

Static Synchronous Compensator (STATCOM) [12] is another PCD that is particularly effective in mitigating voltage sags and supporting grid stability under fluctuating wind conditions. However, its high cost and complexity are a deterrent, especially in small- to medium-sized wind energy installations [13]. Thyristor-Controlled Series Capacitor (TCSC) [14] improves PQ by controlling line impedance. However, while TCSC enhances system stability and power transfer, it is less motivated by reactive power compensation and voltage regulation, making it less suitable for direct voltage stabilization in WECS applications.

DSTATCOMs [15] are a variation of STATCOM explicitly designed for distribution networks. They provide dynamic voltage support by injecting reactive power into the distribution grid. DSTATCOMs are widely used to enhance voltage stability, power quality, and grid reliability, particularly in distribution systems with renewable energy integration. However, like STATCOMs, they can be costly and complex to implement, especially for large-scale wind energy systems [16]. Recently, DVRs [17] have emerged as one of the most effective solutions for mitigating voltage disturbances such as sags, swells, and harmonic distortions in PMSG-based WECS.

Unlike other power conditioning devices, DVRs focus primarily on voltage stability by injecting or absorbing active and reactive power as needed. Their fast dynamic response makes them highly effective in addressing sudden voltage drops caused by wind variability or grid disturbances. Additionally, DVRs are cost-effective, relatively simple to implement, and do not require extensive maintenance, making them an ideal choice for PMSG-based systems that require reliable LVRT capabilities [18].

Generally, DVRs require a control approach for efficiently managing the voltage disturbances and for ensuring that the restored voltage remains within acceptable limits for the connected load. These control approaches assure that DVR responds to sudden variations in the power system, reducing the impact and duration of voltage disturbances. Fuzzy Logic Controllers (FLC) are robust to system uncertainties and parameter variations, offering effective functioning under varying conditions. However, tuning the membership functions and rules is complicated. Thereby, poor tuning degrades the performance. Moreover, less accurate voltage compensation occurs due to inherent imprecision in FLC [19, 20].

Artificial Neural Networks (ANN) manage complex patterns and nonlinear relationships in power systems, which aids in accurate voltage correction in DVR. The lack of transparency is regarded as the major drawback; also, poor generalization occurs due to the improper regularization of data [21, 22]. By integrating the strengths of fuzzy and ANN, ANFIS provides robust control with learning abilities. The parameters of ANFIS affect the system's ability directly to model complex relationships, and hence, these parameters require tuning procedures. Tuning ANFIS parameters helps in refining the model's accuracy and precision in handling voltage disturbances, which is critical for the correct operation of DVRs [23, 24].

The Lower Switch MLI is based on the usual CHBMLI methodology. As a result, the Multi-level Inverter's size and cost will be decreased while maintaining all of the advantages of CHB-MLI and using reduced components. A control strategy is essential for managing switch activities in MLI [25]. Fewer power electronics components are used in the Multi-level inverter design, and the circuitry needed to implement the control techniques is simple. Because of this, the inverter will be tiny, lightweight, reasonably priced, and appropriate for both high- and low-voltage applications [26].

In contrast to these existing conventional solutions, which have limitations in dynamic response, complexity, and cost, the proposed system introduces a Seagull-optimized Type 2 ANFIS controller, offering superior adaptability and faster convergence for managing voltage disturbances in PMSG-based WECS. Additionally, the deployment of a 31-level CHBMLI ensures high-quality AC output with significantly reduced THD, addressing the critical need for improved power quality in grid integration. These innovations differentiate the proposed approach from existing methods by providing a more efficient, cost-effective, and reliable solution for voltage regulation and LVRT enhancement in wind systems. The contributions are as follows:

- A novel approach to improving LVRT capabilities in PMSG-WECS by deploying a DVR with a Seagull-optimized Type 2 ANFIS controller, ensuring enhanced voltage stability and dynamic response to grid disturbances.
- The use of a 31-level CHBMLI with a PI controller to achieve high-quality AC output with reduced THD, improving PQ and system reliability.
- The proposed solution mitigates the voltage fluctuations and disturbances caused by wind variability, ensuring better integration of PMSG-based systems into the grid.

The paper is divided into the following sections: Part 2 describes the proposed technique, Part 3 discusses system modeling, Part 4 presents the results and discussion, and Part 5 concludes the work.

2. Proposed Methodology

To solve the difficulties in integrating RESs with WECS into the contemporary electrical grid, a complete plan has been designed, as seen in Figure 1. To keep the grid stable, the LVRT capability needs to be improved in accordance with fluctuating and intermittent RESs. The incorporation of strategic components has made this feasible.

A sophisticated and efficient technology has been developed to incorporate wind energy into the electrical grid and preserve grid stability even in the circumstances of disruptions and voltage dips. A WECS with a PMSG is used to convert wind energy into electrical power. The system integrates a DVR attached to a super capacitor, which acts as an energy storage device to energize the DVR setup. This guarantees a consistent supply of AC power to the grid, hence reducing voltage fluctuations. Most significantly, a Type 2 ANFIS Controller automatically regulates the DVR's input voltage in response to variations in the entire system. The PWM rectifier converts the AC supply into DC, and the transformer refines the power output by increasing the voltage.

The isolated flyback converter ensures electrical isolation and modifies voltage levels. Following that, the 31-Level CHBMLI receives the regulated output from the Flyback converter. Complex, high-quality AC power is produced from DC electricity via an inverter by producing several voltage levels, minimizing harmonics, and lowering output voltage variations. The PI controller at the grid side sends control signals to the 31-Level CHBMLI. It uninterruptedly monitors the power to ensure accurate control. These signals alter the inverter's functioning to maintain the required voltage and frequency, enabling reliable and efficient synchronization with the grid.

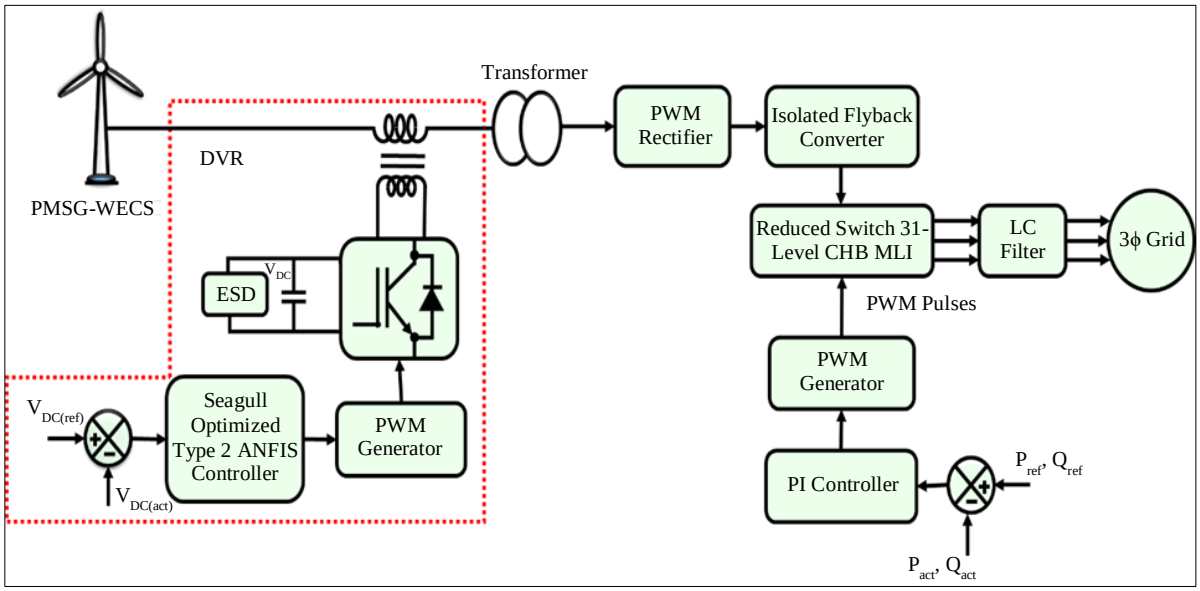

Fig. 1 The proposed PMSG-WECS with DVR

The 31-Level CHBMLI receives accurate control inputs from the PI controller, which constantly monitors actual and reactive power. These power signals regulate the operation of an inverter to maintain the required voltage and frequency, which improves grid synchronization and reliability. This all-encompassing technology basically ensures that grid requirements are met while also enhancing grid stability when renewable energy sources are integrated.

3. System Modelling

3.1. Wind Energy Turbine System with PMSG

The proposed wind system includes a wind turbine, surface magnet-type PMSG, corresponding controllers for converters on the grid and generator sides, DC-link capacitance, LCL filter, coupling transformers, synchronization relays, and the utility grid. Subheadings 1 through 4 show the wind turbine and PMSG dynamic simulations.

3.1.1. Dynamic Modeling of PMSG

The PMSG has a smaller pole pitch and is suitable for low-speed applications since it uses a permanent magnet in place of an excitement winding. v_{dm} and v_{qm} stand for the d- and q-axis stator voltages.

$$v_{dm} = R_a i_{dm} + \omega_r L_q i_{qm} - L_d p i_{dm} \quad (1)$$

$$v_{qm} = -R_a i_{qm} - \omega_r L_d i_{dm} + \omega_r \lambda_r - L_q p i_{qm} \quad (2)$$

Where, i_{dm} and i_{qm} are the stator currents on d- and q-axes, respectively, and R_a represents per-phase stator winding resistance; ω_r represents the dq reference frame's speed; The d- and q-axis stator inductances are denoted by L_d and $L_q$respectively, Relative to the rotor flow, λ_r age; the derivative operator is represented by $p = d/dt$.

$$L_d = L_{Is} + L_{dm} \tag{3}$$

$$L_q = L_{Is} + L_{qm} \tag{4}$$

Where, $L_{Is}$is the stator winding leakage inductance and L_{dm} and L_{qm}indicates d- and q-axis magnetizing inductances, respectively. The electromagnetic force produced by the PMSG (T_e) can be written as follows:

$$T_e = 1.5P\left[i_{qm}\lambda_r - i_{dm}i_{qm}\left(L_d - L_q\right)\right] \tag{5}$$

Where P is the number of pole pairs.

3.1.2. Modeling of Wind Turbine

The following relationship between wind's kinetic power (P_w) and turbine mechanical power(P_M):

$$P_M = P_w C_p = \frac{1}{2}\rho A_T v_w^3 C_p \tag{6}$$

Where, ρ is the air density and C_p is the wind turbine's power coefficient. $AT = \pi r^2 T$ Swept area of the turbine blade, r_T wind turbine blade length; the wind speed is represented by v_w. To achieve the optimal value of the power coefficient $C_{p,OPT}$and the extraction of the maximum possible wind power, the wind turbine blade's Tip Speed Ratio (TSR) λ_T should be adjusted based on variations in wind speeds. The TSR $\lambda_{T,OPT}$ optimal value is described as follows:

$$\lambda_{T,OPT} = \frac{\omega_{T,OPT} r_T}{v_w} \tag{7}$$

Where, $\omega_{T,OPT}$ is the wind turbine's optimal angular speed. Reliability and power quality are increased when a wind energy turbine system with a PMSG and DVR for LVRT is used. This guarantees steady grid operation during voltage disruptions.

3.2. LVRT by DVR

In particular, for critical loads, the DVR is the most effective solution for averting interruptions caused by power dip. DVR, as shown in Figure 2, operates in standby mode unless there are unusual network conditions.

The nominal voltage is maintained constant at the load side by the DVR, which also provides the voltage differential between the lines during voltage sag. It can be used, in general, to protect important loads by averting sudden voltage shifts.

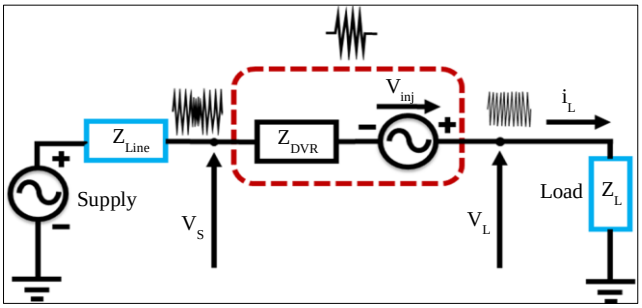

Fig. 2 Equivalent circuit diagram of DVR

Voltage Source Inverter (VSI), energy storage, bypass thyristor, injection transformers, protection circuits, and passive filters make up the DVR. It uses the transformer to introduce a voltage series (V_{inj}) into the network whenever there is a voltage sag or rise. Consequently, it is possible to keep load voltage at its nominal level. The voltage that was injected is stated below.

$$V_L = V_s + V_{inj} \tag{8}$$

Where, V_L, V_s and V_{inj}indicates injected voltages, the sagging supply, and the load, respectively. Under suitable voltage conditions, the load power of each phase is,

$$S_L = V_L I_L^* = P_L - jQ_L \tag{9}$$

Where, I_LLoad current and P_L and $Q_L$active and reactive powers during sags and swells. When the intended voltage is returned to normal by the DVR, Equation (2) can be written as follows.

$$S_L = P_L - jQ_L = (P_S - jQ_S) + \left(P_{inj} - jQ_{inj}\right) \tag{10}$$

3.2.1. Operation Modes

Three modes of operation are available to the DVR: injection, standby and protection.

Mode of Protection

This mode of operation protects the DVR against high load-side current exceeding a tolerable threshold. The DVR may sustain damage as a result of this high current, which results from load-side issues. In order to prevent these fault currents, the DVR must be shielded. The thyristors and breakers typically create a distinct channel that can be used to do this. If this path is not considered, an overvoltage occurs inside the injection transformers.

Standby Mode$\left(V_{inj} = 0\right)$

In this mode of operation, DVR does not inject electricity due to the absence of abnormalities detected. Therefore, the bypass switch avoided the DVR to prevent any minor voltage injection. The reduced voltage winding of the injection transformer is bypassed using the VSI as soon as a voltage disturbance is detected.

Injection Mode$(V_{inj} > 0)$

In this operating mode, in the event that a voltage disturbance is detected, the DVR switches from standby mode to this mode. Next, through the injection transformer, the DVR injects the desired voltage until the voltage is fully decreased and returned to a healthy state. In the proposed system, a supercapacitor is employed as the Energy Storage Device (ESD) alongside the DVR. The choice of a supercapacitor is based on its ability to provide rapid energy discharge, high power density, and extended cycle life, which are crucial for maintaining voltage stability in PMSG-based WECS under fluctuating conditions.

The selected supercapacitor has a capacity of 500 F at 48 V, which allows it to store and discharge energy efficiently to support the DVR during voltage disturbances. The supercapacitor is directly connected to the DC link of the DVR, where it serves as a buffer to absorb energy during grid fluctuations or disturbances and releases it when required to maintain the voltage level. This setup is designed to ensure smooth energy exchange, where the supercapacitor discharges its stored energy into the DVR to compensate for sudden voltage drops. It charges back from the grid when normal voltage conditions are restored. The integration of the supercapacitor with the DVR provides a significant advantage in handling transient voltage disturbances. In wind energy systems, voltage instability caused by fluctuating wind conditions leads to interruptions and poor grid synchronization. However, by utilizing a supercapacitor, the proposed system injects the required voltage compensation to mitigate these fluctuations. This capability enhances the system's LVRT performance, ensuring grid stability even under severe voltage dips.

3.3. Seagull Optimized Type 2 ANFIS Controller for DVR

This hybrid approach combines the adaptive learning capabilities of the ANFIS model with the optimization power of the Seagull Optimization Algorithm (SOA), aiming to enhance the effectiveness of voltage compensation in power systems using DVR. Initialization in SOA involves setting up the initial positions of seagulls in the search space, representing the ANFIS parameters. For Type 2 ANFIS, initialization includes configuring fuzzy membership functions, neural network weights, and control-related parameters, providing a starting point for subsequent optimization, such as through the Seagull algorithm, to enhance system performance. Initialization of the Type 2 ANFIS controller involves defining the fuzzy membership functions and initializing the neural network weights.

$$\mu_{A_i}(x) = exp\left(-\frac{(x-C_i)^2}{2\sigma_i^2}\right) \quad (11)$$

Where C_i is center and σ_i is the width of the fuzzy membership function, A_i They are associated with a linguistic variable. The neural network weights are initialized using random values or some systematic approach based on the network architecture. In a simple two-layer neural network with weights w_{ij}, is randomly initialized. The objective function evaluates the performance of the Type 2 ANFIS controller. This function captures the effectiveness of the controller in compensating for voltage disturbances in the DVR system. The parameters of the algorithm are listed in Table 1, and the flowchart for the proposed Seagull optimized ANFIS is shown in Figure 3.

Table 1. Parameters of Seagull optimized type 2 ANFIS

Parameters	Values
Population Size	30
Maximum Iterations	100
f_c	2
Number of Inputs to ANFIS	2
Number of Fuzzy Membership Function	3
Type of membership function	Gaussian
Number of Fuzzy Rules in ANFIS	9
Learning Rate	0.01
Optimization Criteria	MSE

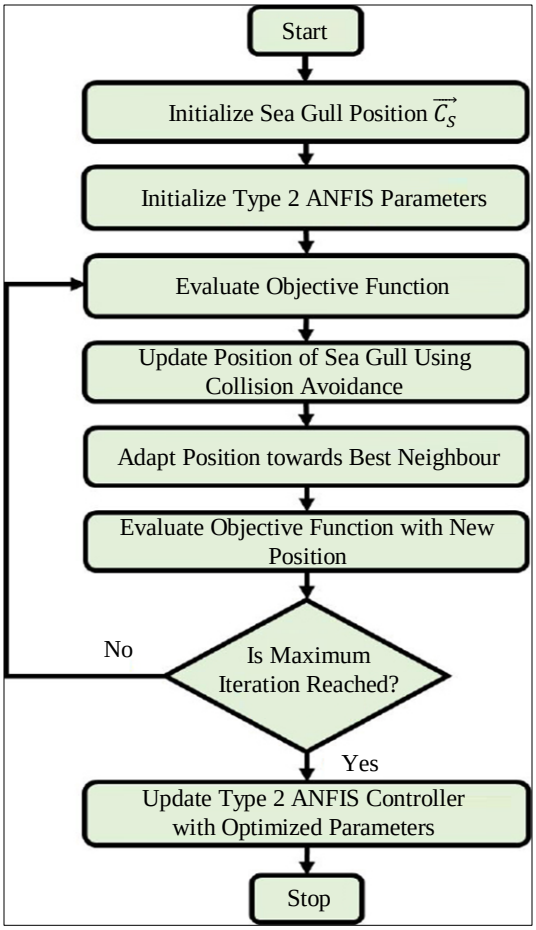

Fig. 3 Flowchart for proposed Seagull optimized ANFIS

3.3.1. Seagull Optimization

The SOA is selected over other optimization methods like GA or PSO due to its ability to balance exploration and exploitation phases more efficiently, which is crucial for avoiding local minima in complex, multi-dimensional optimization problems. Unlike GA, which tends to focus heavily on global exploration in its early stages, and PSO, which suffers from premature convergence, SOA dynamically adjusts its control parameters, providing a more adaptive search mechanism that better handles the highly non-linear and dynamic characteristics of voltage disturbances in power systems. Moreover, SOA is particularly suitable for applications where fast convergence is necessary, as it combines collision avoidance and movement toward the best solution, ensuring faster adjustments during the optimization process.

In SOA, the optimization process is inspired by the behavior of seagulls as they search for food. Seagulls typically exhibit two main behaviors: collision avoidance (to avoid crowding and overlapping with other seagulls) and movement toward a better food source (adapting to the best solution). These behaviors are analogous to the exploration and exploitation phases in traditional optimization techniques. SOA balances between these phases dynamically to avoid local minima and ensure faster convergence. Initialization in SOA involves setting up the initial positions of seagulls in the search space, which correspond to the initial ANFIS parameters. These positions are randomly assigned within the solution space, and each position represents a potential solution to the optimization problem.

For Type 2 ANFIS, initialization includes configuring fuzzy membership functions, neural network weights, and control-related parameters, providing a starting point for subsequent optimization using the Seagull algorithm to enhance system performance. The position of a seagull, represented by $\overrightarrow{C_s}$ corresponds to the current set of ANFIS parameters. To avoid collisions with neighboring solutions, the updated equation,

$$\overrightarrow{C_s} = A \times \overrightarrow{P_s}(t) \tag{12}$$

Where A specifies the control variable that dynamically adjusts based on the iteration count (t). The control variable A is defined as

$$A = f_c - (t \times \left(\frac{f_c}{Max\_iteration}\right)) \tag{13}$$

Where, f_c is a constant parameter, and $Max\_iteration$ is the maximum iteration count. To adapt towards the better neighbour, the seagull adjusts its position $\overrightarrow{C_s}$ in the direction of the best neighbor's position $\overrightarrow{P_{bs}}(t)$. This update is influenced by a control variable B, and the equation is given by,

$$\overrightarrow{M_s} = B \times (\overrightarrow{P_{bs}}(t) - \overrightarrow{P_s}(t)) \tag{14}$$

$$B = 2 \times A^2 \times rand \tag{15}$$

Where $rand$ is a random value between 0 and 1.

The seagull combines collision avoidance and movement towards the optimal individual to reach a new location $\overrightarrow{D_s}$. The new position $\overrightarrow{D_s}$ is determined by adding the collision avoidance update $\overrightarrow{C_s}$ and the adaptation to the best neighbour update $\overrightarrow{M_s}$, resulting in an equation,

$$\overrightarrow{D_s} = \overrightarrow{C_s} + \overrightarrow{M_s} \tag{16}$$

After the SOA converges and produces the final set of optimized parameters $\overrightarrow{D_s}$, the next step is to update the Type 2 ANFIS controller with these optimized parameters. The Type 2 ANFIS controller incorporates fuzzy membership functions, neural network weights, and other control parameters. By adjusting fuzzy membership functions with optimized parameters from the SOA, the approach effectively regulates DVR, demonstrated by its ability to mitigate voltage sags, swells, and interruptions. The iterative optimization ensures adaptability to dynamic conditions, making it well-suited for maintaining voltage quality and stability. Switching losses are decreased, and overall system efficiency is increased when the Sea Gull Optimized Type 2 ANFIS Controller is used in conjunction with reduced switch 31-Level MLI in DVR.

3.4. Isolated Flyback Converter

An Isolated Flyback converter is a type of power supply topology commonly used for low power applications. It is called "Flyback" because it stores energy in the magnetic field of the transformer during the first half of the switching cycle (when the primary side transistor is on) and then transfers that energy to the output during the second half of the cycle (when the transistor is off). Isolation is achieved through the transformer, which permits the turn's ratio to determine if the output voltage is higher or lower than the input. This makes the Flyback converter appropriate for situations requiring galvanic separation, such as in many consumer electronics, industrial controls, and automotive systems.

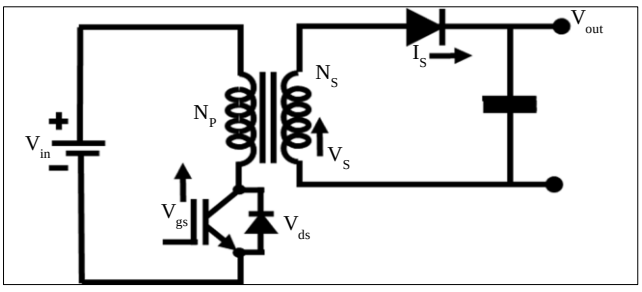

Fig. 4 Configuration of isolated flyback converter

Flyback converters are known for their simplicity and low cost, but they have limitations in comparison to others in terms of power management and efficiency. The isolated converter topologies, like forward converters or push-pull converters, are shown in Figure 4. They are typically used in applications where these limitations are acceptable, such as in low-power AC-DC adapters, battery chargers, and LED drivers.

3.5. Reduced Switch 31-Level MLI

The rectified output from the wind is processed via an Isolated Flyback converter before it reaches the 31-level CHBMLI reduction switch. This converter not only ensures voltage level adjustments but also provides electrical isolation. The Isolated Flyback converter's output is fed to 31-Level CHBMLI, which is mostly in charge of transforming its DC power into excellent AC power.

The introduction of an isolated flyback converter enables the proposed configuration to decrease the quantity of combined DC sources, hence streamlining the design. Thirty one voltage levels are generated by the combined action of the switches related to polarity generation (T_1, T_2, T_3 *and* T_4) and level generation (S_1, S_2, S_3 *and* S_4). While switches T_3 and T_4 are in use during the negative half cycle, T_1 and T_2 are activating a positive half cycle.

Interestingly, a zero voltage level was obtained by deactivating all level generation switches. This arrangement guarantees the intended multilayer features of the inverter by enabling efficient control and manipulation of the output voltage levels.

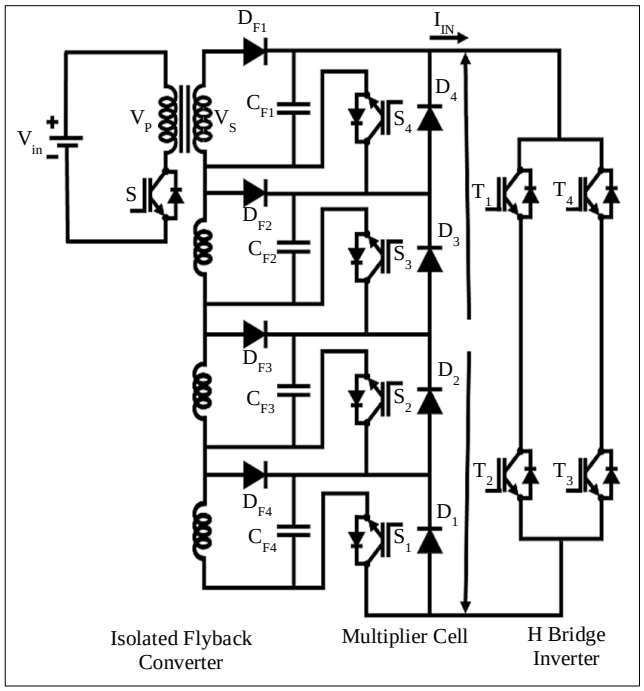

Table 2. Switching operations of switch 31-level MLI

S_1	S_2	S_3	S_4	**Output Voltage**
1	1	1	1	$V_{S1} + V_{S2} + V_{S3} + V_{S4}$
0	1	1	1	$V_{S2} + V_{S3} + V_{S4}$
1	0	1	1	$V_{S1} + V_{S3} + V_{S4}$
0	0	1	1	$V_{S3} + V_{S4}$
1	1	0	1	$V_{S1} + V_{S2} + V_{S4}$
0	1	0	1	$V_{S2} + V_{S4}$
1	0	0	1	$V_{S1} + V_{S4}$
0	0	0	1	V_{S4}
1	1	1	0	$V_{S1} + V_{S2} + V_{S3}$
0	1	1	0	$V_{S2} + V_{S3}$
1	0	1	0	$V_{S1} + V_{S3}$
0	0	1	0	V_{S3}
1	1	0	0	$V_{S1} + V_{S2}$
0	1	0	0	V_{S2}
1	0	0	0	V_{S1}
0	0	0	0	0
1	0	0	0	$-V_{S1}$
0	1	0	0	$-V_{S2}$
1	1	0	0	$-(V_{S1} + V_{S2})$
0	0	1	0	$-V_{S3}$
1	0	1	0	$-(V_{S1} + V_{S3})$
0	1	1	0	$-(V_{S2} + V_{S3})$
1	1	1	0	$-(V_{S1} + V_{S2} + V_{S3})$
0	0	0	1	$-V_{S4}$
1	0	0	1	$-(V_{S1} + V_{S4})$
0	1	0	1	$-(V_{S2} + V_{S4})$
1	1	0	1	$-(V_{S1} + V_{S2} + V_{S4})$
0	0	1	1	$-(V_{S3} + V_{S4})$
1	0	1	1	$-(V_{S1} + V_{S3} + V_{S4})$
0	1	1	1	$-(V_{S2} + V_{S3} + V_{S4})$
1	1	1	1	$-(V_{S1} + V_{S2} + V_{S3} + V_{S4})$

For the design of MLI, ideal switching operation is assumed, where switches operate with negligible transition times and losses. This simplifies the analysis by ignoring the effects of switching transients and losses. Moreover, the converter and inverter are assumed to operate without significant thermal issues under normal operating conditions. Conduction happens through D_2, D_3, and D_4 in the positive half cycle when switch S_1 is turned ON. When the optional system is operating, Table 2 shows the switching operations and matching output voltage levels. Conduction moves to D_1, D_3

and D_4, with the switch S_2 set ON, resulting in output as the positive half cycle transitions to mode 2.

Switches are turned on in the order listed, continuing this pattern of sequential switching throughout the 15 modes. Next, the negative half cycle is switched using the same sequence of switches. The PI controller generates control signals for the inverter while continually monitoring real and reactive power. This ensures exact control over output without any interruptions during the wind farm's smooth integration with the grid.

The proposed system, which uses 31-Level CHBMLI for PMSG-based WECS, aids in enhancing LVRT capabilities with the integration of DVR. This setup generates reduced THD and mitigates the voltage stability issues in spite of varying environmental circumstances.

3.6. Environmental and Economic Impacts of the Proposed Solution

The proposed system supports the efficient integration of renewable energy, particularly wind energy, into the power grid. By enhancing LVRT capabilities and reducing THD, the system minimizes interruptions and enhances the reliability of RESs. This increased reliability enables greater penetration of wind energy, leading to a reduction in dependence on fossil fuels and a corresponding decrease in greenhouse gas emissions. Furthermore, improved voltage stability reduces stress on grid infrastructure, which extends the lifespan of grid components and reduces the frequency of maintenance and replacements, thereby contributing to environmental sustainability.

From the economic perspective, the integration of a high-efficiency inverter and optimized control strategies minimizes harmonic content, which reduces wear and tear on electrical components. This leads to lower maintenance and replacement costs, especially for critical grid equipment. The improved LVRT capabilities and rapid voltage compensation provided by the DVR reduce grid instability and prevent downtime. This is particularly beneficial for wind farm operators, who can avoid revenue losses associated with grid disconnections or equipment failures. Moreover, the reduction in THD results in higher efficiency and lower energy losses during transmission. This improvement translates into cost savings over time, as less energy is wasted due to distortions in the power waveform.

4. Results and Discussion

MATLAB simulation was used to validate the optimized system precisely. The efficacy performance of each system component has been assessed by in-depth research and modelling. Table 3 establishes the key specification parameters required for the design of the proposed system. The sections that follow provide in-depth research findings and discussions.

Table 3. Parameters specification

Specification	Rating
PMSG-Wind System	
No. of Turbines	1
Stator Resistance	0.975Ω
Power	$10kw$
Voltage	575V
PMSG Inductance	$0.01H$
Flux Linkage	$0.91Wb$
Pole Pairs	3
Air Density	$1.218kg/m^2$
Base Wind Speed	$12m/s$
Pitch Angle Beta	$2degree$
DC Link Capacitor	$1500\mu F$
DVR	
Series Voltage Injection	$100v$
Filter Inductance	$2.7mH$
Grid Voltage	$415V$
Filter Capacitance	$50\mu F$
Line Inductance	$0.5mH$
Line Resistance	0.1Ω
Switching Frequency	$10KHz$

4.1. Under Sag Condition

Figure 6 shows the responses of a PMSG under a voltage sag condition. Figures 6(a) and 6(b) demonstrate the voltage and current profile of the PMSG system, respectively, when there is voltage sag. The phenomenon, which lasts between 0.2 and 0.3 seconds, is caused by the generator being impacted by an unusual wind direction.

Furthermore, Figure 6(c) shows the in phase waveform under voltage sag conditions. This graphic depiction makes it possible to examine in great detail how the PMSG system reacts to voltage sag, providing important insights into its dynamic properties under such unfavorable electrical circumstances.

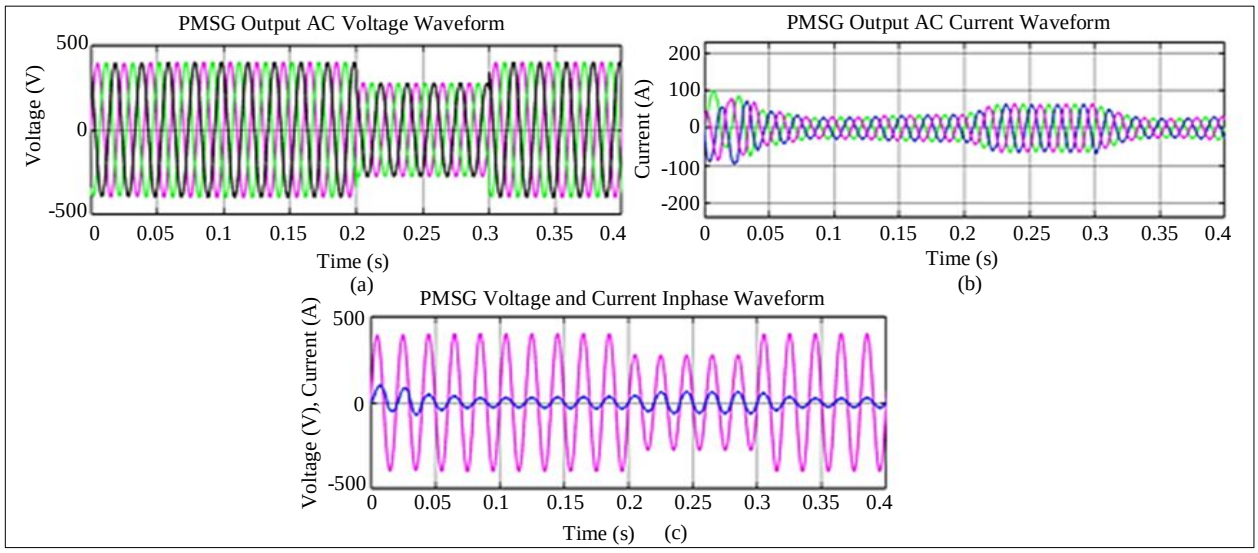

Fig. 6 PMSG response to voltage sag: (a) Voltage profile, (b) Current dynamics, and (c) Voltage and current in phase waveform.

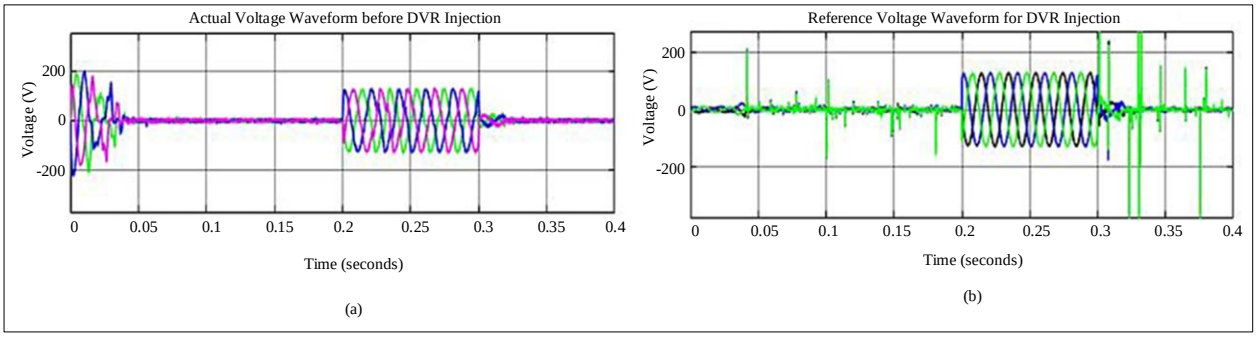

Fig. 7 (a) Actual voltage waveform before DVR injection, and (b) Reference voltage waveform for DVR injection.

An important part of minimizing a voltage sag scenario is the use of DVR. The first phase in Figure 7(a) shows a scenario in which there are strong oscillations prior to the injection of DVR assistance. The detrimental consequences of voltage sag on the system are blamed for these oscillations. On the other hand, Figure 7(b) shows the reference voltage that DVR injected following installation. The voltage sag problems that have been noticed are much reduced as a result of reference voltage injected by DVR. By increasing voltage support, stabilizing the system, and lessening the effect of the voltage sag, this mitigation is accomplished. The efficiency of DVR support in reducing the negative impacts of voltage sag in the system is demonstrated by a comparison of the conditions before and after DVR injection.

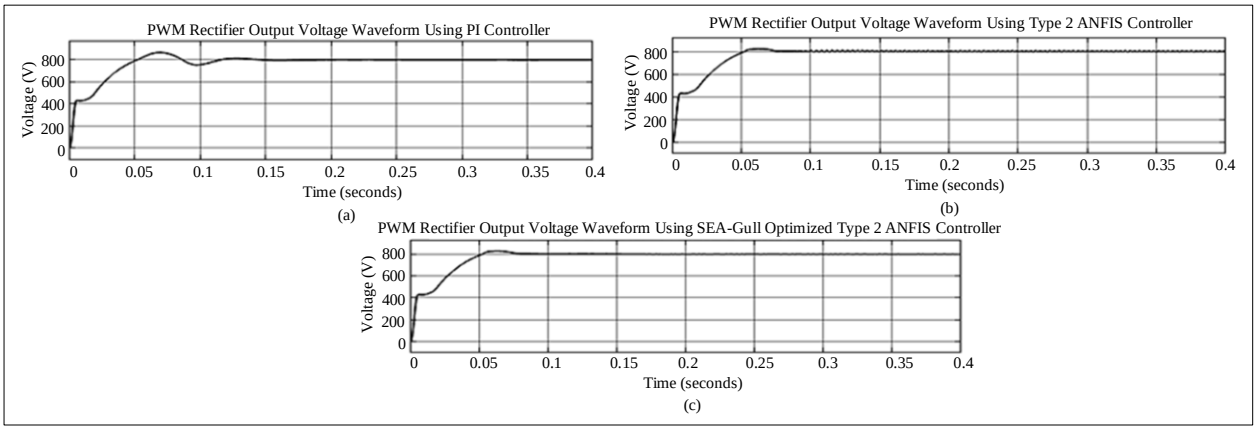

Fig. 8 PWM rectifier output voltage waveform using (a) PI controller, (b) Type 2 ANFIS controller, and (c) Seagull optimized Type 2 ANFIS controller for sag condition.

Figure 8 shows the voltage stability performance of the PI controller, Type 2 ANFIS, and Seagull optimized Type 2 ANFIS controller. In all cases, the voltage is maintained at 800V and settles within 0.2 seconds. Notably, the Seagull optimized Type 2 ANFIS controller achieves stability in just 0.1 seconds without any distortion, as shown in Figure 8(c).

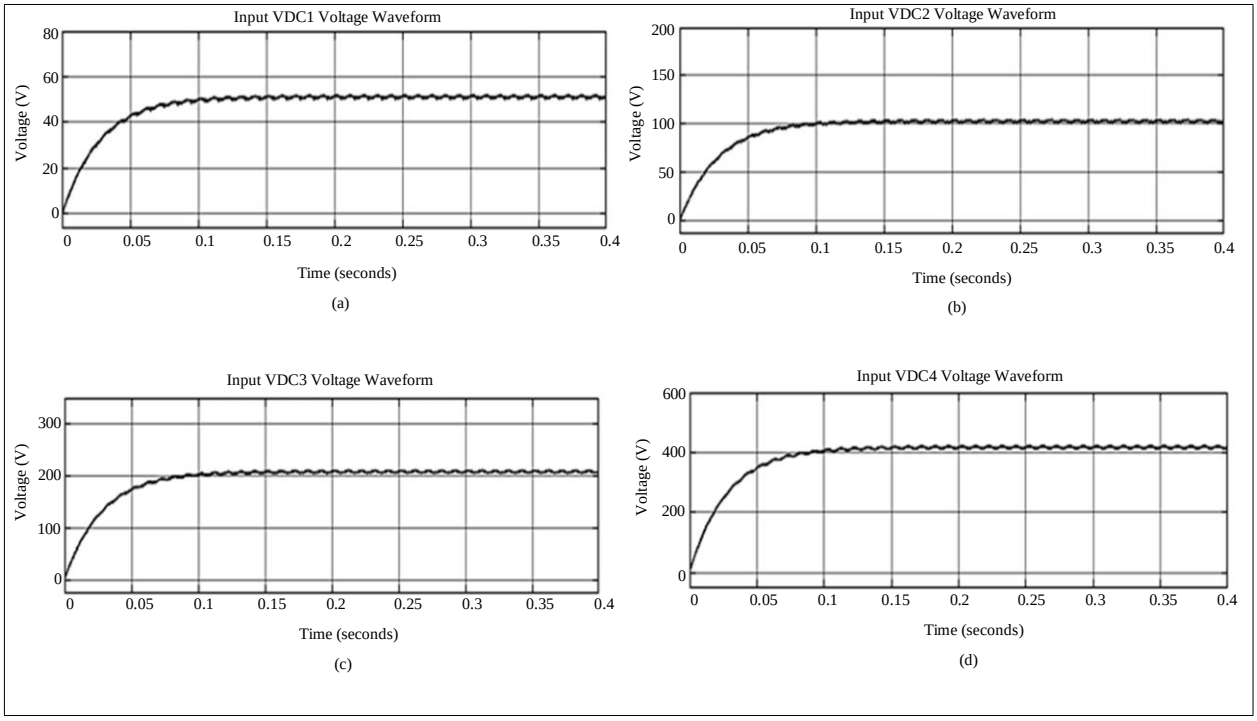

Fig. 9 Flyback converter output voltage waveform

The Flyback converter significantly alters the DC link voltage, as illustrated in Figure 9, which depicts the voltage sag state and demonstrates four voltage stages. The voltage gradually increases from 50V to 100V, 200V, and ultimately 400V. Each stage enhances the effectiveness of the 31-level MLI by serving a specific function. This voltage variation allows the system to adapt to different operational conditions and requirements of the connected load.

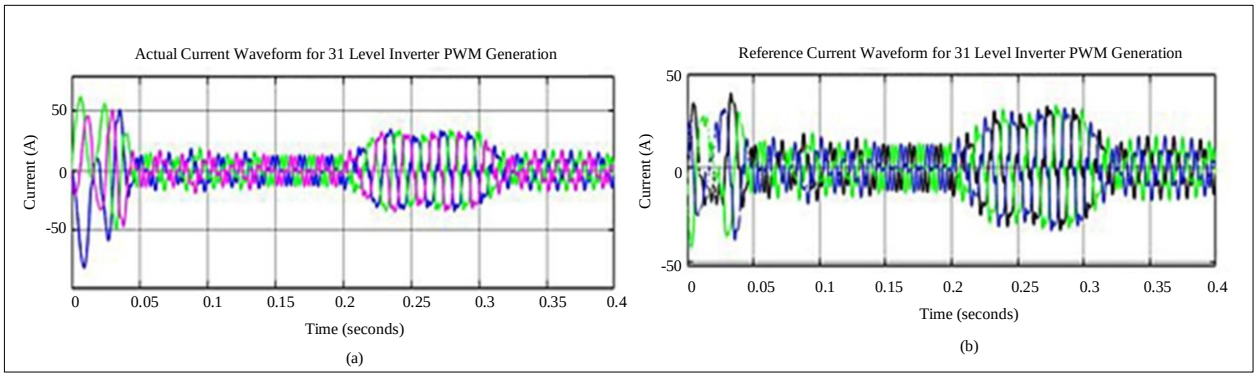

Fig. 10 (a) Actual current waveform, and (b) Reference current waveform.

In the context of the 31-level MLI system, Figure 10 provides an overview of the actual and reference current characteristics. The actual current waveform is depicted in Figure 10(a), which demonstrates the MLI's operational behavior in real time. Figure 10(b), on the other hand, shows the reference current, which stands for the intended current levels that the MLI seeks to attain.

Figure 11 illustrates the output waveforms of 31-Level MLI during a voltage sag. Figure 11(a) highlights the ability of the system to lessen the effects of voltage sag for maintaining a stable voltage supply. At the same time, Figure 11(b) shows the output current profile, demonstrating the system's capability to deliver steady current despite voltage fluctuations.

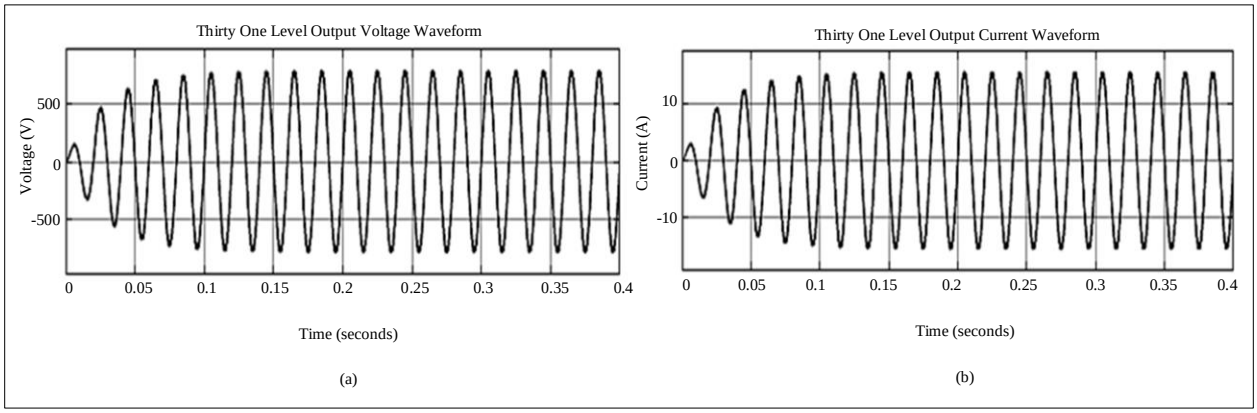

Fig. 11 Thirty one level output (a) Voltage waveform, and (b) Current waveform.

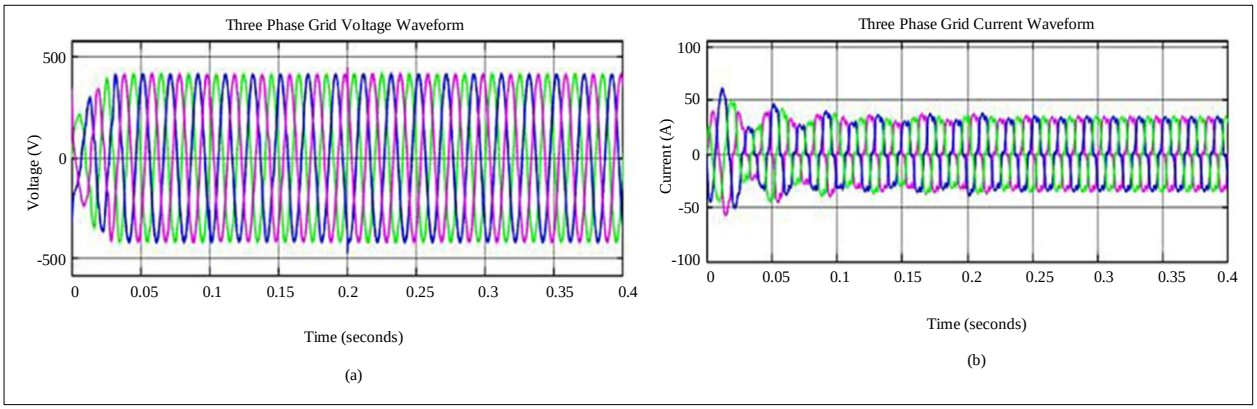

Fig. 12 Three phase (a) Voltage, and (b) Current waveform.

The waveform of 3Φ grid using the proposed system's influence is shown in Figure 12. The grid voltage waveform is shown in Figure 12(a), demonstrating the voltage's stable state. The stabilized outcome of the proposed system shows the successful reduction of voltage sag problems, which guarantees a steady voltage to grid load.

Figure 12(b) shows that grid current has a stable current value. Figure 13 provides a comprehension of the power characteristics of the proposed system under operational settings by illustrating the dynamics of both real and reactive power waveforms. The reactive power waveform shows how well the system can sustain voltage levels, but the real power waveform shows how much power the system actually uses. The comprehensive perspective of the system's power behavior provided by these waveforms, when combined, makes it easier to assess the system's effectiveness and performance.

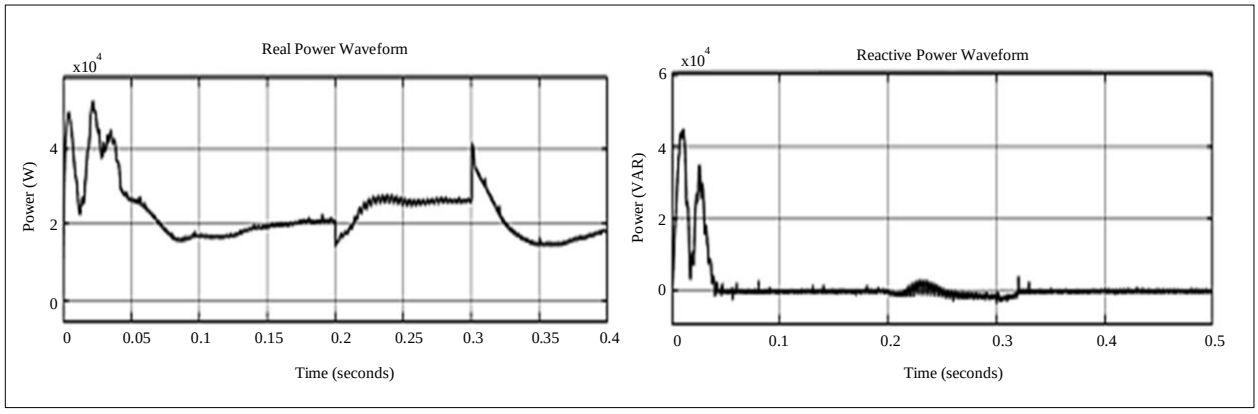

(a) (b)

Fig. 13 (a) Real power waveform, and (b) Reactive power waveform.

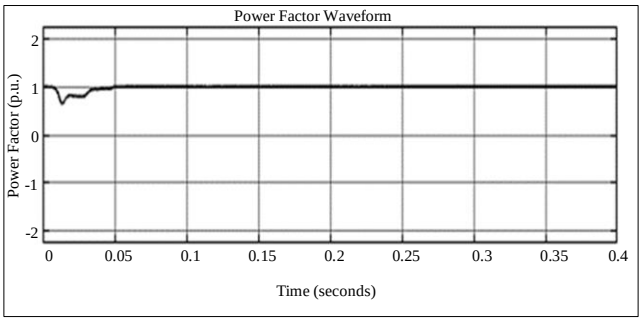

Fig. 14 Power factor waveform

The power factor waveform is depicted in Figure 14, where the steady-state level is consistently reached at 1 per unit (1 P.U.). The system's power factor is continuously modified and optimized through a dynamic process where the power factor waveforms gradually rise. This dynamic adjustment enhances the performance and efficacy of the power system by making sure it operates at maximum capacity while minimizing losses.

4.2. Under Swell Condition

Figure 15 illustrates the reaction of the PMSG system during a voltage swell. With regard to the voltage waveform, Figure 15(a) shows how the voltage swell condition between 0.2s and 0.3s impacts the voltage output of the system. Comparatively, in Figure 15(b), the current sheds light on how the system behaved electrically in reaction to the voltage peak. Furthermore, Figure 15(c) reveals the historical representation of voltage and current.

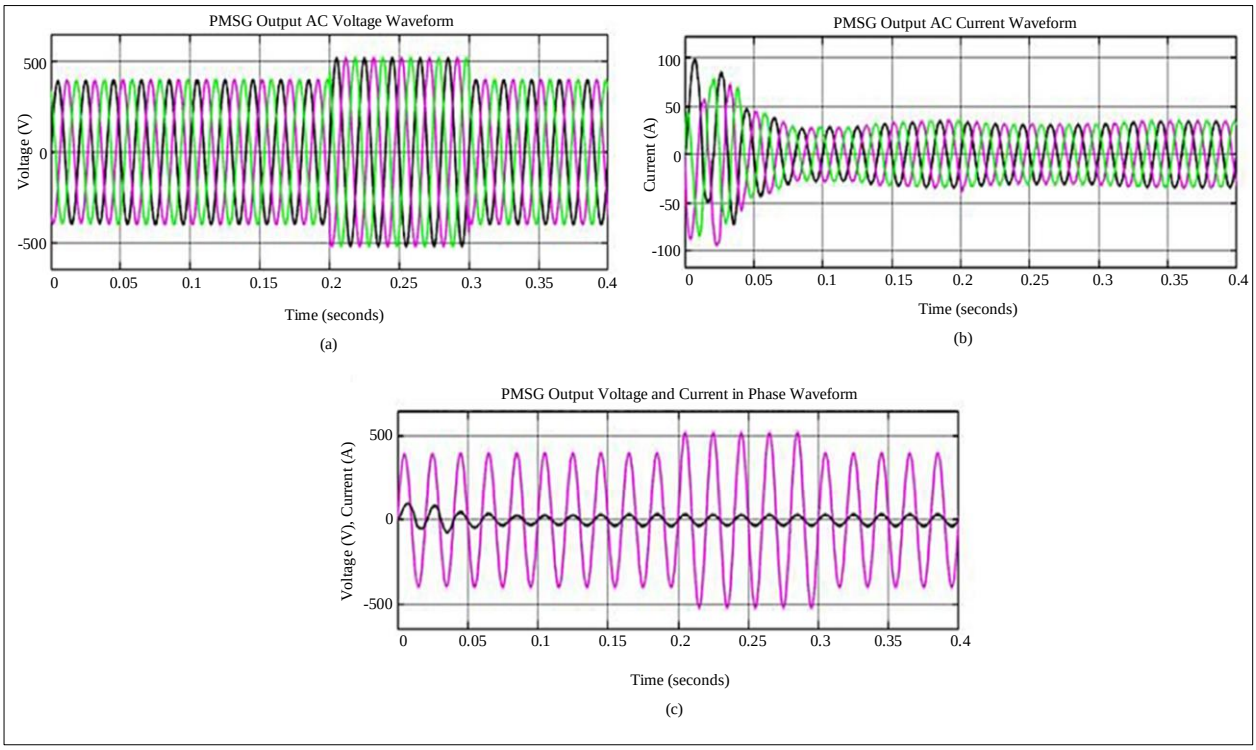

Fig. 15 PMSG (a) Output AC voltage waveform, (b) Output AC current waveform, and (c) Output voltage and current in phase waveform.

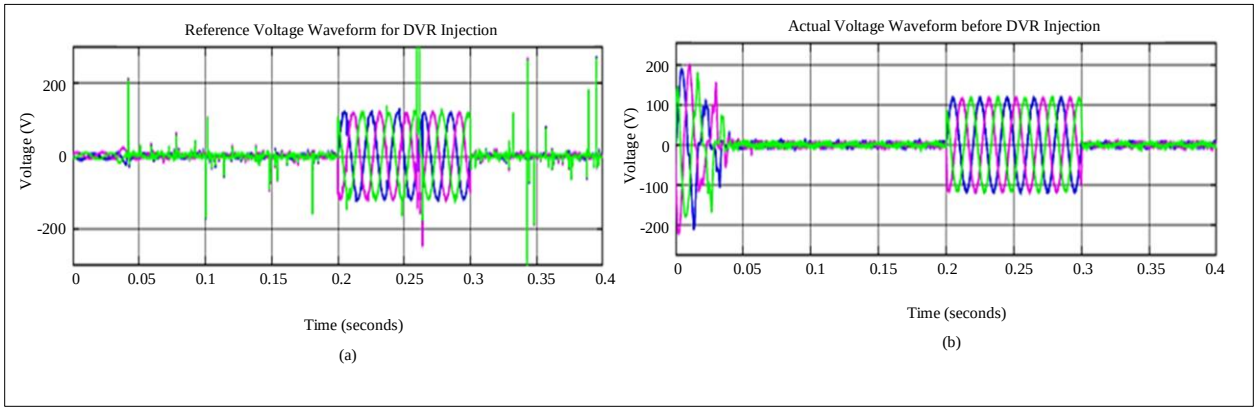

Fig. 16 DVR Injection (a) Reference voltage, and (b) Actual voltage.

The use of DVR is crucial to reducing a voltage swell scenario. Figure 16(a) denotes the reference voltage, whereas Figure 16(b) indicates the actual voltage before DVR injection. The reference voltage appears to have a stable segment with minimal fluctuations and a swell period centered around 0.25 to 0.3 seconds. The waveform suggests that this is the ideal voltage level that the system aims to maintain. With these injected waveforms, the issues of voltage swell are rectified.

Figure 17 depicts the voltage stability performance of three different control systems: a PI controller, a Type 2 ANFIS controller, and a Seagull optimized Type 2 ANFIS controller.

In all three cases, voltage is maintained at 800V and settles at a time variation of 0.2s. However, it is noteworthy that the Seagull optimized Type 2 ANFIS controller settles even faster, at 0.1s, without any distortion.

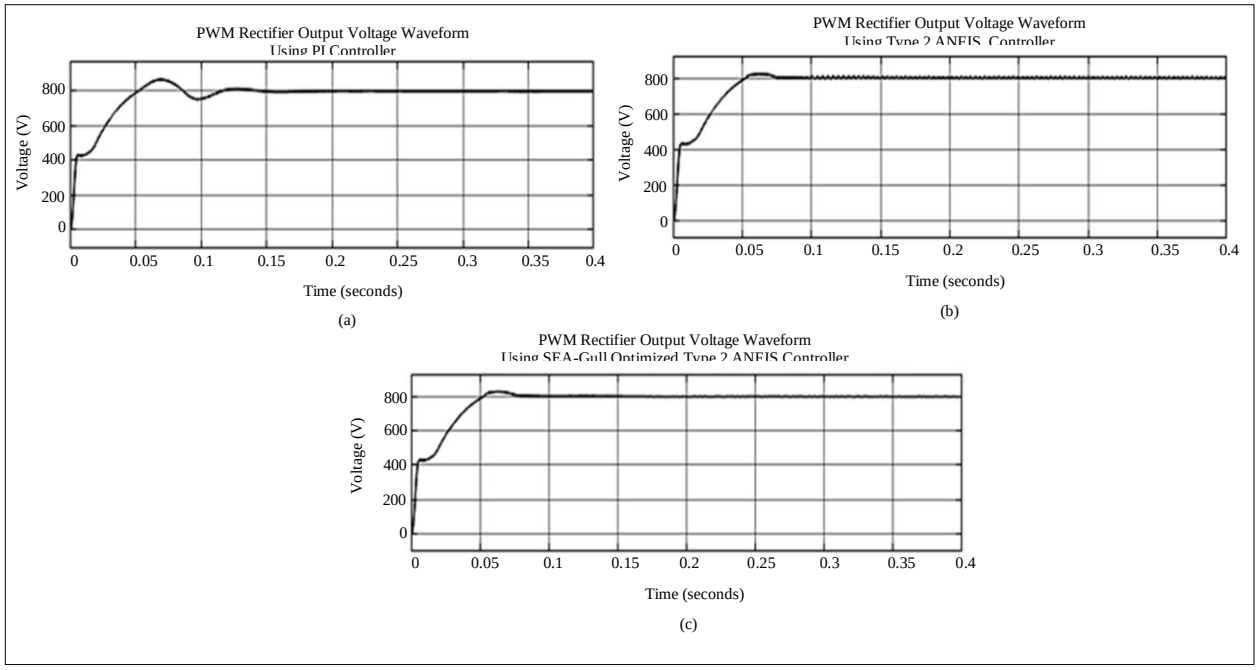

Fig. 17 PWM rectifier output voltage waveform using (a) PI controller (b) Type 2 ANFIS controller, and (c) Seagull optimized Type 2 ANFIS controller for swell condition.

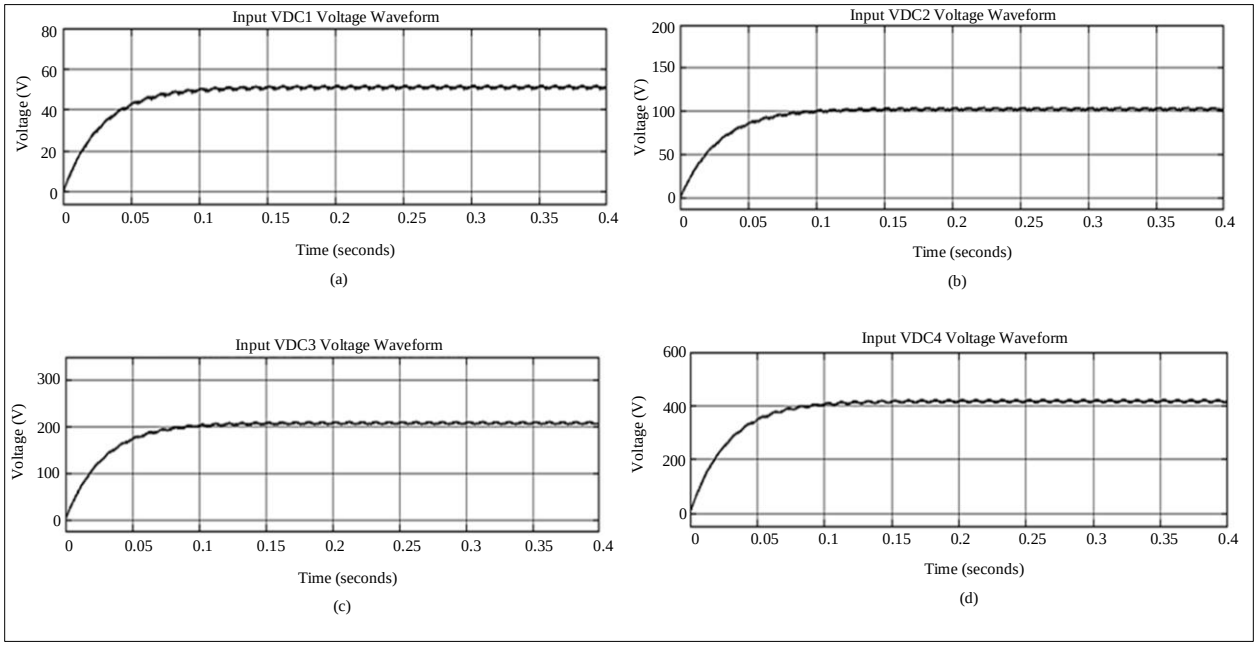

Fig. 18 Flyback converter output voltage waveform

The Flyback converter makes critical changes to the DC link voltage, which is shown in Figure 18 as resembling the voltage swell state and provides voltage in four stages. The voltage steadily rises from 50V to 100V, 200V, and 400V in ultimate terms. Every level contributes to the effectiveness of the 31-level MLI by fulfilling a certain function. The voltage variation enables the system to adjust to various operational situations and requirements within the linked load.

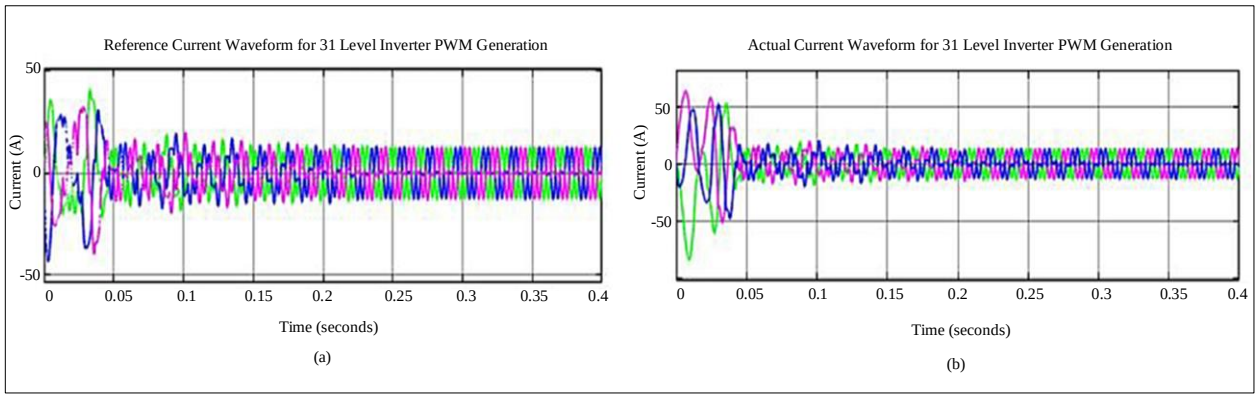

Fig. 19 31 Level Inverter PWM generator for (a) Reference current, and (b) Actual current waveform.

Figure 19 represents the effect of DVR on current dynamics and current stability. The reference current is shown in Figure 19(a), emphasizing oscillations and fluctuations. On the other hand, the stabilizing effect brought about by DVR injection is shown in Figure 19(b), which shows the actual current. Following DVR intervention, the actual current exhibits increased stability and decreased oscillations, highlighting the correcting effect of DVR on the current waveform. This graphic illustrates how effective DVR is in improving the current in system's stability and performance.

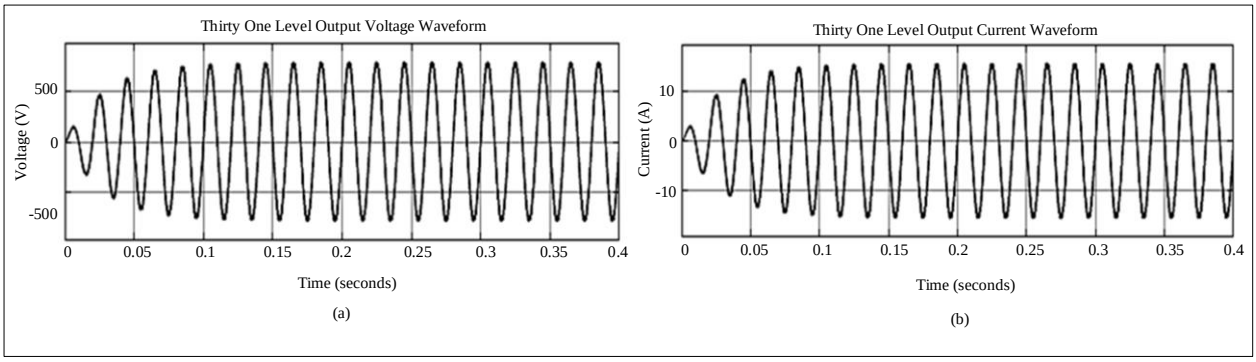

Fig. 20 Thirty One level output (a) Voltage waveform, and (b) Current waveform.

Figure 20 shows the 31-Level MLI's output voltage and current waveforms during voltage swell. With regard to the stabilized output voltage, Figure 20(a) highlights the system's capacity to reduce voltage swell and preserve a steady voltage supply. Concurrently, Figure 20(b) displays a matching output current profile, demonstrating the system's capacity to provide consistent current even in the presence of voltage fluctuations. This analysis demonstrates the proposed system's ability to adjust to swell conditions and guarantee dependable power distribution to linked loads.

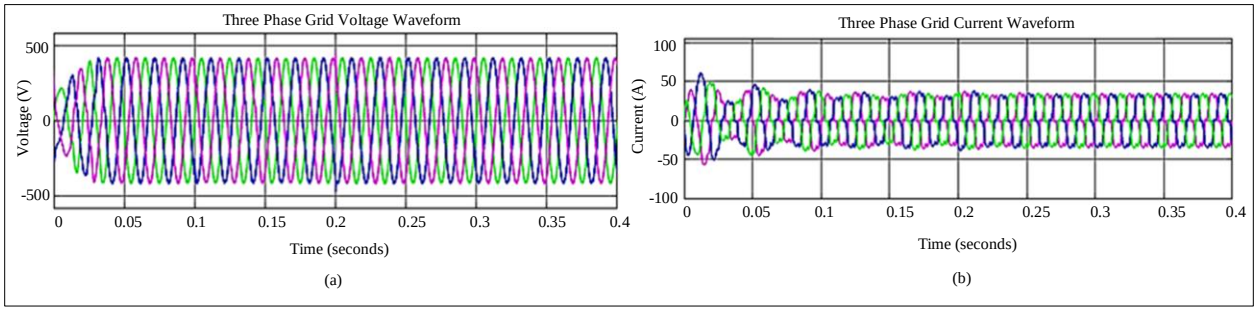

Fig. 21 Three phase Grid (a) Voltage waveform, and (b) Current waveform.

Figure 21 shows how the proposed solution affects the grid dynamics within a 3Φ grid. The load voltage waveform is shown in Figure 21(a) with clarity, illustrating the system's ability to stabilize voltage by handling voltage swell problems. Figure 21(b) shows the grid current waveform concurrently, demonstrating a constant and regulated current level. The capability of the system to support stability is crucial for the dependable functioning of the grid, highlighting the benefits of the proposed approach in reducing voltage swell and guaranteeing grid load continuity.

Figure 22 presents power dynamics, including both reactive and actual power waveforms. The real power consumption seen in Figure 22(a) shows the actual power waveform.

Figure 22(b) shows the reactive power waveform concurrently, which shows a non-reactive power component oscillating between the source and load. Evaluating the effectiveness and efficiency of the system in providing power to the attached load requires a thorough understanding of the dynamics of actual and reactive power.

The graph in Figure 23 illustrates the power factor waveform, with 1 per unit (1 P.U.) being the steady-state level that is continuously reached. Power factor waveforms gradually rise as a result of a dynamic process that continuously modifies and optimizes the system's power factor. By ensuring that the power system runs at total capacity while reducing losses, this dynamic adjustment helps to improve the power system's performance and efficiency.

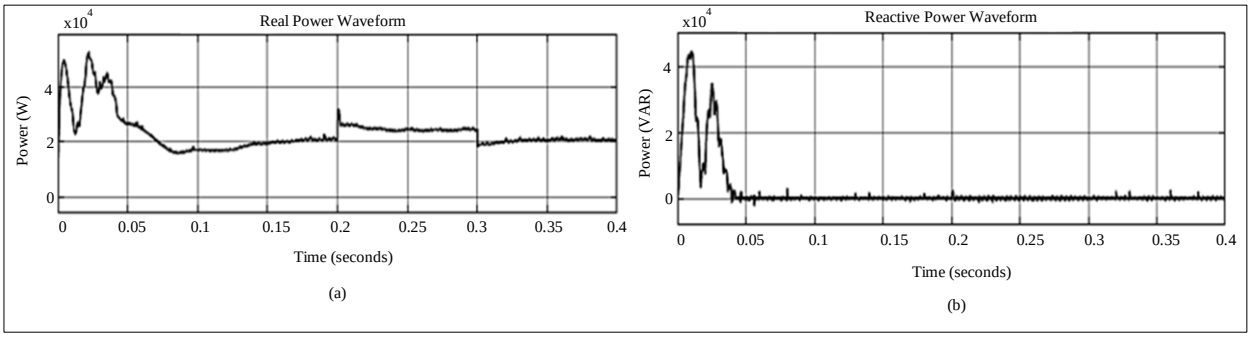

Fig. 22 (a) Real, and (b) Reactive power waveform.

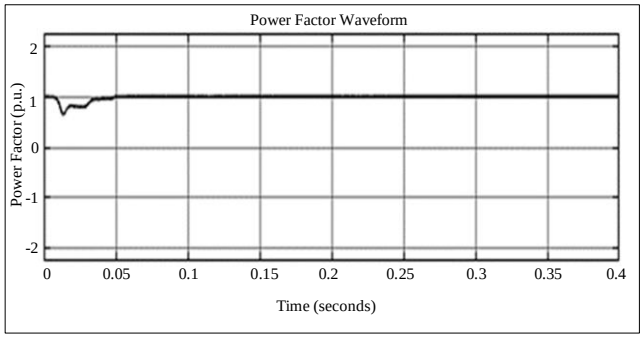

Fig. 23 Waveform of power factor

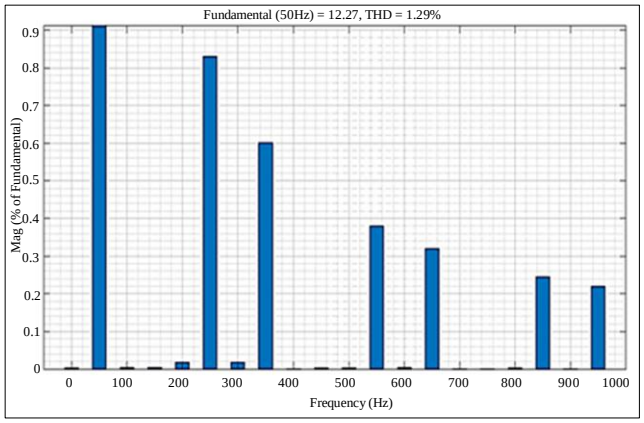

Fig. 24 THD waveform

The THD value, which is 1.29%, is shown in Figure 24. This low THD result highlights the effectiveness of the power signal produced by the proposed configuration, indicating that there is minimal harmonic distortion in the system's output.

Table 4. Comparison of THD analysis

Techniques	THD (%)
Modified DVR [27]	7.85
TransZSI-DVR with IMCBC [28]	4.89
Fuzzy controller based DVR [19]	1.98
ANFIS controller based DVR [23]	2.01
ARO based DVR [29]	2.3
Proposed controller	1.29

Table 4 represents the comparison of THD analysis of the proposed control with multiple methods, including Modified DVR, TransZSI-DVR with IMCBC, Fuzzy based DVR, ANFIS based DVR and ARO based DVR, which come out to be 7.85%, 4.89%, 1.98%, 2.01%, 2.3%and 1.29% respectively. In comparison, the proposed optimized method performs at its best when compared to other approaches and has a lower THD score of 1.29%.

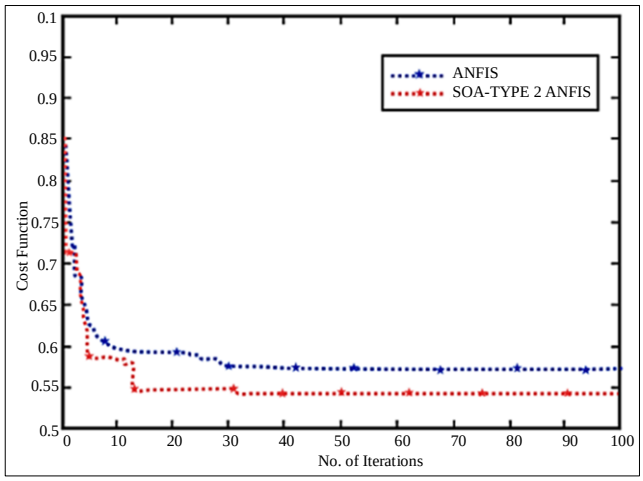

Fig. 25 Cost function comparison

The cost function comparison between an ANFIS controller and T2-ANFIS for optimal DVR control is presented in Figure 25. T2-ANFIS outperforms standard adaptive neuro fuzzy inference system controllers in terms of performance while achieving a reduced cost. The T2-ANFIS controller is shown to be better than conventional fuzzy control methods in this chart, which also provides useful information about how well it optimizes DVR control while reducing associated expenses.

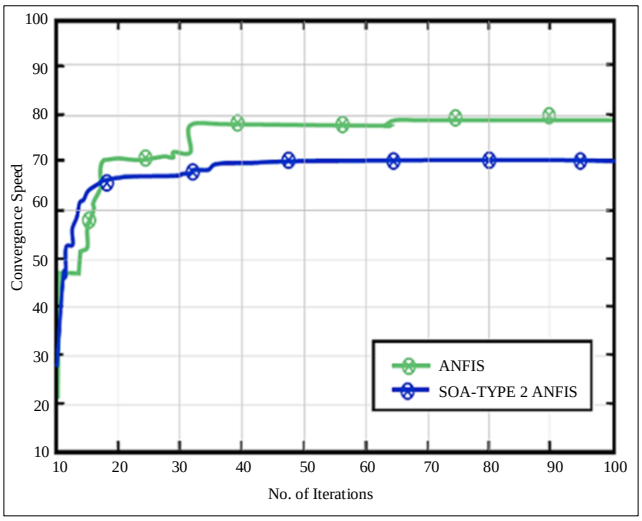

Fig. 26 Convergence speed comparison

Figure 26 compares the ANFIS controller and the T2-ANFIS controller in terms of convergence speed. The comparison demonstrates the faster convergence speed at minimum no. of iterations attained by the type 2 adaptive neural fuzzy inference system controller and its superior convergence dynamics optimization performance over the traditional ANFIS. This figure offers important information about the effectiveness and efficiency of the proposed controller in guaranteeing quicker convergence for better control results.

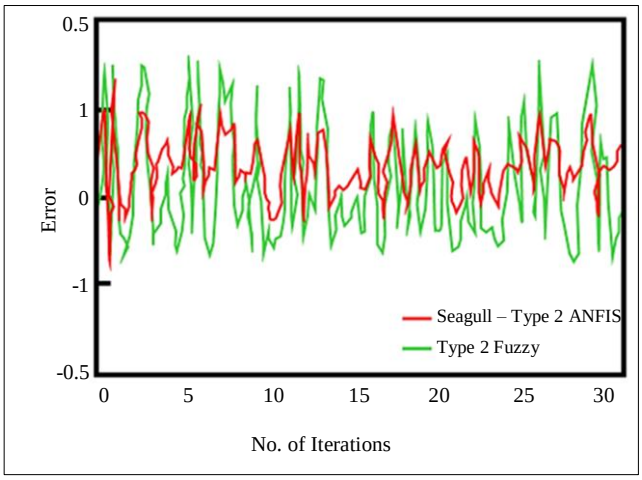

Fig. 27 Comparison of error

The comparison of error between Type 2 Fuzzy and Seagull optimized Type 2 ANFIS is shown in Figure 27. The attained outcomes clearly demonstrate that the optimized control generates highly accurate outputs, thereby exhibiting reduced error values for varying numbers of iterations.

The proposed system achieves better results compared to existing techniques due to precise control enabled by the Seagull-optimized Type 2 ANFIS controller, the superior waveform quality produced by the 31-Level CHBMLI, and the rapid voltage stabilization provided by the DVR with integrated energy storage. The combination of these innovations results in lower THD, improved LVRT performance, faster response times, and a cost-effective solution for enhancing wind energy integration. These advantages position the proposed system as a robust and efficient solution for addressing the challenges of integrating renewable energy into modern power grids.

4.3. Implementation Limitations

The proposed system faces certain challenges in real-world implementation. Grid compatibility and compliance with varying standards complicate integration, while the high initial cost of advanced components like DVRs and multilevel inverters affect economic viability. Scalability to smaller installations, real-time performance, and computational demands pose technical limitations.

Environmental factors and system reliability are concerns, as extreme conditions require additional protective measures and regular maintenance, particularly in offshore or remote installations. Effective communication and monitoring infrastructure is essential for real-time control, but this is costly and difficult in remote areas.

Integrating the system with older infrastructure requires significant upgrades, and the inclusion of energy storage systems introduces its own set of challenges. Moreover, regulatory and policy constraints also limit adoption, requiring

careful navigation of local energy codes and grid operator requirements. Addressing these challenges is crucial for the successful and widespread deployment of the proposed system in practical wind energy applications.

4.4. Future Works

Future work focuses on enhancing the Seagull-optimized Type 2 ANFIS controller with alternative optimization techniques, which improves real-time performance and adaptability. Expanding the system to hybrid RES, such as combining wind and solar power, increases its versatility. Further integration of advanced energy storage solutions, such as lithium-ion batteries, and improved energy management strategies optimize performance under varying conditions.

The system's adaptability to other RESs, such as solar or hydroelectric power, will also be explored. Incorporating smart grid technologies and distributed control strategies enhances real-time grid integration capabilities. Real-world testing and case studies are essential to validate practical performance and identify potential limitations. Additionally, efforts to reduce costs and improve scalability for smaller wind farms, along with environmental and economic impact assessments, are crucial for broader adoption.

5. Conclusion

This research presents a potential solution to challenges associated with the integration of PMSG-WECS in modern power grids, specifically in addressing LVRT capabilities. The incorporation of DVR significantly enhances the reliability and stability of the grid by mitigating voltage dip disturbances. The integration of the Type 2 ANFIS controller dynamically adjusts to changing grid conditions, thereby improving the system against disturbances and voltage fluctuations. The rectified output is processed by an isolated flyback converter and a 31-level MLI, which supports reducing harmonic distortion and voltage variations. The validation outcome reveals that the proposed system effectively boosts the LVRT capabilities by maintaining a THD of 1.29%, ensuring compliance with grid standards. By addressing the critical issue of LVRT, the proposed system facilitates the seamless integration of wind energy into the power grid and supports the resilience and reliability of power infrastructure.

Acknowledgements

We thank the Department of Science and Technology (DST), New Delhi for providing India-Slovenia Joint Research Project.

References

[1] Amirhossein Sajadi et al., "Guest Editorial: Special Issue on Recent Advancements in Electric Power System Planning with High-Penetration of Renewable Energy Resources and Dynamic Loads," *International Journal of Electrical Power and Energy Systems*, vol. 129, 2021. [CrossRef] [Google Scholar] [Publisher Link]

[2] Mohammad Mohammadi, and Ali Mohammadi, "Empowering Distributed Solutions in Renewable Energy Systems and Grid Optimization," *Distributed Machine Learning and Computing*, vol. 2, pp. 141-155, 2024. [CrossRef] [Google Scholar] [Publisher Link]

[3] Ruban Periyanayagam Antonysamy et al., "Performance Enhancement Using Robust Sliding Mode Approach-Based Current Control for PMVG-WECS," *IEEE Transactions on Industrial Electronics*, vol. 70, no. 10, pp. 10156-10166, 2022. [CrossRef] [Google Scholar] [Publisher Link]

[4] Adel Sotoudeh, and Mohammad Mahdi Rezaei, "An Adaptive Control Strategy for Grid-Forming of SCIG-Based Wind Energy Conversion Systems," *Energy Reports*, vol. 10, pp. 114-122, 2023. [CrossRef] [Google Scholar] [Publisher Link]

[5] Malathi Panner Selvam, Subha Karuvelam Palraj, and Gnana Sundari Madasamy, "Adaptive Control of a Single Source Reduced Switch MLI-Based DSTATCOM for Wind Energy Conversion System," *Electrical Engineering*, vol. 106, pp. 5269-5290, 2024. [CrossRef] [Google Scholar] [Publisher Link]

[6] Rupak Datta, and Young Hoon Joo, "Fuzzy Memory Sampled-Data Controller Design for PMSG-Based WECS with Stochastic Packet Dropouts," *IEEE Transactions on Fuzzy Systems*, vol. 31, no. 12, pp. 4421-4434, 2023. [CrossRef] [Google Scholar] [Publisher Link]

[7] Joseba Lopez-Mendia et al., "Improving the Owc Wave Energy Converter Power Take-Off Efficiency Throughout Experimental and Numerical Characterisation of an SCIG," *Energies*, vol. 17, no. 5, 2024. [CrossRef] [Google Scholar] [Publisher Link]

[8] Hamid Chojaa et al., "Robust Control of DFIG-Based WECS Integrating an Energy Storage System with Intelligent MPPT Under a Real Wind Profile," *IEEE Access*, vol. 11, pp. 90065-90083, 2023. [CrossRef] [Google Scholar] [Publisher Link]

[9] Yazdan H. Tabrizi, and M. Nasir Uddin, "Multi-Agent Reinforcement Learning-Based Maximum Power Point Tracking Approach to Fortify PMSG-Based WECSs," *IEEE Transactions on Industry Applications*, 2024. [CrossRef] [Google Scholar] [Publisher Link]

[10] Vinay Kumar Awaar et al., "Dynamic Voltage Restorer–A Custom Power Device for Power Quality Improvement in Electrical Distribution Systems," *In Proceedings Power Quality: Infrastructures and Control*, Springer, Singapore, pp. 97-116, 2023. [CrossRef] [Google Scholar] [Publisher Link]

[11] Muhammad Ruswandi Djalal, Imam Robandi, and Mohammad Almas Prakasa, "Stability Enhancement of Sulselrabar Electricity System Using Mayfly Algorithm Based on Static Var Compensator and Multi-Band Power System Stabilizer PSS2B," *IEEE Access*, vol. 11, pp. 57319-57340, 2023. [CrossRef] [Google Scholar] [Publisher Link]

[12] Priyanka Priyadarsini, Avik Bhattacharya, and Muneer V., "A Novel SMC Integrated WECs for Wind Farm Commitment Implementing Battery Storage System," *IEEE Transactions on Industry Applications*, pp. 1-14, 2024. [CrossRef] [Google Scholar] [Publisher Link]

[13] Jun-Hao Chen, Kuang-Hsiung Tan, and Yih-Der Lee, "Intelligent Controlled DSTATCOM for Power Quality Enhancement," *Energies*, vol. 15, no.11, 2022. [CrossRef] [Google Scholar] [Publisher Link]

[14] Subodh Kumar Mohanty et al., "An Enhanced Protective Relaying Scheme for TCSC Compensated Line Connecting DFIG-Based Wind Farm," *IEEE Transactions on Industrial Informatics*, vol. 20, no. 3, pp. 3425-3435, 2023. [CrossRef] [Google Scholar] [Publisher Link]

[15] Kuang-Hsiung Tan, Meng-Yang Li, and Xiang-Yu Weng, "Droop Controlled Microgrid with DSTATCOM for Reactive Power Compensation and Power Quality Improvement," *IEEE Access*, vol. 10, pp. 121602-121614, 2022. [CrossRef] [Google Scholar] [Publisher Link]

[16] Sathish Babu Pandu et al., "Power Quality Enhancement in Sensitive Local Distribution Grid Using Interval Type-II Fuzzy Logic Controlled DSTATCOM," *IEEE Access*, vol. 9, pp. 59888-59899, 2021. [CrossRef] [Google Scholar] [Publisher Link]

[17] Saeed Daneshvar Dehnavi et al., "Dynamic Voltage Restorer (DVR) with a Novel Robust Control Strategy," *ISA transactions*, vol. 121, pp. 316-326, 2022. [CrossRef] [Google Scholar] [Publisher Link]

[18] Ahmad Eid et al., "Improvement of Active Distribution Systems with High Penetration Capacities of Shunt Reactive Compensators and Distributed Generators Using Bald Eagle Search," *Ain Shams Engineering Journal*, vol. 13, no. 6, 2022. [CrossRef] [Google Scholar] [Publisher Link]

[19] B. Samhitha, and T. Gowri Manohar, "Performance Analysis of Fuzzy Logic Controller Based DVR for Power Quality Enhancement," *International Journal of Scientific Research in Science and Technology*, vol. 10, no. 1, pp. 462-71, 2023. [CrossRef] [Google Scholar] [Publisher Link]

[20] O. Jeba Singh, and D. Prince Winston, "Enhanced Method of Mitigating Voltage Sags and Swells Using Optimized Fuzzy Controlled DVR," *Iranian Journal of Science and Technology, Transactions of Electrical Engineering*, vol. 47, no. 1, pp. 147-158, 2023. [CrossRef] [Google Scholar] [Publisher Link]

[21] Arjun Joshi et al., "Comparative Analysis of Dynamic Voltage Restorer Based on PI and ANN Control Strategies in Order to Improve the Voltage Quality Under Non-Linear Loads," *World Journal of Advanced Research and Reviews*, vol. 22, no. 3, pp. 292-303, 2024. [CrossRef] [Google Scholar] [Publisher Link]

[22] Meet R. Patel, and Amit Vilas Sant, "ANN-Based Reference Voltage Generation Scheme for Control of Dynamic Voltage Restorer," *International Journal of Social Ecology and Sustainable Development (IJSESD)*, vol. 13, no. 2, pp. 1-16, 2022. [CrossRef] [Google Scholar] [Publisher Link]

[23] Abdallah Ben Abdelkader, Youssef Mouloudi, and Mohammed Amine Soumeur, "Integration of Renewable Energy Sources in The Dynamic Voltage Restorer for Improving Power Quality Using ANFIS Controller," *Journal of King Saud University-Engineering Sciences*, vol. 35, no. 8, pp. 539-548, 2023. [CrossRef] [Google Scholar] [Publisher Link]

[24] Prashant Kumar et al., "Performance Evaluation of GRNN And ANFIS Controlled DVR Using Machine Learning in Distribution Network," *Optimal Control Applications and Methods*, vol. 44, no. 2, pp. 987-1005, 2023. [CrossRef] [Google Scholar] [Publisher Link]

[25] Shaik Reddi Khasim et al., "A Novel Asymmetrical 21-Level Inverter for Solar PV Energy System with Reduced Switch Count," *IEEE Access*, vol. 9, pp. 11761-11775, 2021. [CrossRef] [Google Scholar] [Publisher Link]

[26] Venu Sonti, Sachin Jain, and Bhagya Sai Kumar Reddy Pothu, "Leakage Current Minimization Using NPC DC Decoupling Method for Three-Phase Cascaded Multilevel PV Inverter," *IEEE Transactions on Circuits and Systems II: Express Briefs*, vol. 67, no. 12, pp. 3247-3251, 2020. [CrossRef] [Google Scholar] [Publisher Link]

[27] Rakeshwri Pal, and Sushma Gupta, "Topologies and Control Strategies Implicated in Dynamic Voltage Restorer (DVR) for Power Quality Improvement," *Iranian Journal of Science and Technology, Transactions of Electrical Engineering*, vol. 44, pp. 581-603, 2020. [CrossRef] [Google Scholar] [Publisher Link]

[28] Ali Moghassemi, Shayan Ebrahimi, and Farzad Ferdowsi, "A Novel Control Scheme for Transzsi-Dvr to Enhance Power Quality in Solar Integrated Networks," *North American Power Symposium (NAPS)*, College Station, TX, USA, pp. 1-6, 2021. [CrossRef] [Google Scholar] [Publisher Link]

[29] Nagwa F. Ibrahim et al., "Enhancing the Functionality of a Grid-Connected Photovoltaic System in A Distant Egyptian Region Using an Optimized Dynamic Voltage Restorer: Application of Artificial Rabbits Optimization," *Sensors*, vol. 23, no. 16, pp. 1-29, 2023. [CrossRef] [Google Scholar] [Publisher Link]